Pulsatile signaling of bistable switches reveal the distinct nature of pulse processing by mutual activation and mutual inhibition loop

Soutrick Das and Debashis Barik*

School of Chemistry, University of Hyderabad, Central University P.O., Hyderabad, 500046, Telangana, India

*Corresponding author, E-mail: dbariksc@uohyd.ac.in

ACCEPTED

Abstract

Cells often encounter various external and internal signals in a non-sustained pulsatile manner with varying amplitude, duration and residual value. However, the effect of signal pulse on the regulatory networks is poorly understood. In order gain a quantitative understating of pulse processing by bistable switches, we investigated pulse induced population inversion kinetics in bistable switches generated either by mutual activation or by mutual inhibition motifs. We show that both a transient intense pulse and a prolonged weak pulse can induce population inversion, however by distinct mechanisms. An intense pulse facilitates the population inversion by reducing the inversion time, while a weak prolonged pulse allows more late responders to flip their steady state causing increased average transition time. Although the inversion is controlled by the pulse amplitude and duration, however the fate of the inverted state is dictated by the residual signal that determines the mean residence at the flipped state. Therefore, population inversion and its maintenance require a proper tuning of all three signal parameters. Bistable system of mutual activation motif is more prone to make a transient response to the pulse however it is less susceptible to flip its steady state. While the bistability of mutual inhibition motif does not make a transient response yet it is more prone to switch its steady state. By comparing the pulse parameters and statistical properties of associated times scales, we conclude that a bistable switch originating from mutual activation loop is less susceptible to spurious signals as compared to the mutual inhibition loop.

Keywords: bistable switch, signal pulse, signal processing, positive feedback loop, robustness

1. Introduction

Living cells receive a plethora of external and internal signals altering the expression of genes required for appropriate cellular response against these signals (Kholodenko, 2006). Signaling pathways carry the information encoded in the signals to the nucleus where specific genes are targeted for their activation or inactivation decoding the signals. Although, the signaling networks can be quite complex with a significantly large number of regulators involved in numerous interconnected chemical reactions, however majority of the signaling networks contain a core regulatory motif that functions as the main engine in processing the signals. Some of these important motifs are signal transducer, feed-forward loop, negative feedback loop, positive feedback loop (Ferrell Jr, 2002; Tyson and Novák, 2010). These networks motifs are capable of generating nontrivial dynamical and steady state responses (Purvis and Lahav, 2013; Tyson and Novak, 2020; Tyson et al., 2003). For example, negative feedback and incoherent feed-forward loops are capable of generating temporal pulse and are found to be key in regulating in adaptation (Ferrell, 2016; Ma et al., 2009; Mangan and Alon, 2003). Negative feedback loop is also a key ingredient for generating temporal oscillations observed in circadian oscillations (Becker-Weimann et al., 2004; Gonze, 2011; Kim and Forger, 2012; Leloup and Goldbeter, 2003; Ueda et al., 2001), cell division cycle (Barik et al., 2016; Chen et al., 2004) and NF-κB pathway (Hayot and Jayaprakash, 2006; Hoffmann et al., 2002). Positive feedback loops are known to generate bistability leading to an abrupt change in activation state or expression of a macromolecular species such as genes and proteins. Bistability plays a key regulatory role in G1 to S phase transition in the mammalian cell (Yao et al., 2008), mitotic control in yeast (Pomerening et al., 2003) and frog egg extracts (Sha et al., 2003), apoptosis (Bagci et al., 2006; Spencer and Sorger, 2011), cellular differentiation (Domingo-Sananes et al., 2015; Wang et al., 2009; Zhang et al., 2014) and biological memory (Ajo-Franklin et al., 2007; Chang et al., 2010; Doncic et al., 2015).

In modeling these network motifs, typically, steady state dose response curves or dynamical properties of the network motifs are analyzed considering the presence of persistent signal (Tyson et al., 2003). However, cells may experience signals in a discrete manner in which the signals appear as train of pulses with varying amplitudes, durations and intervals and due to the variation of these parameters the signal may appear as noisy (Raj and van Oudenaarden, 2008). There are many examples of pulsatile signaling specific distinct gene expression and subsequent cellular response in various organisms. For example, in *Saccharomyces cerevisiae* proteomic analysis revealed pulsatile dynamics of several transcription factors (Dalal et al., 2014). Particularly, the transcription factor Msn2 was found to exhibit, under glucose

ACCEPTED

starvation, dose dependent pulsatile dynamics regulating expressions of several genes depending on its temporal expression pattern (Hansen and O'Shea, 2016). Radiation induced DNA damage induces p53 pulses and differential cellular fates emerge depending on the features of pulses (Harton et al., 2019; Purvis et al., 2012). In epithelial cells, epidermal growth factor concentration dependent modulation of ERK pulses is required for the proliferation of these cells (Albeck et al., 2013). Pulsatile temporal ERK activity was found to be key in diversification of cellular fates in *Caenorhabditis elegans* (de la Cova et al., 2017). Temporal oscillations in the expression of transcription factors Ascl1 and Hes1 are required for the maintenance of multipotency in the mouse neural progenitor cells, whereas sustained expression of Ascl1 leads to differentiation (Imayoshi et al., 2013; Ochi et al., 2020). Correlation between the pulses of NF-κB and differential gene expression patterns have been identified in the recent past (Lane et al., 2017; Zambrano et al., 2016). Subsequently, mathematical model studies revealed the topology of network motifs that are capable of generating pulses (Gao et al., 2018; Lormeau et al., 2021; Martinez-Corral et al., 2018; Zhang et al., 2016). Therefore, it is important to gain a systematic quantitative understanding of how various network motifs process pulsatile signals such that regulatory units process it as a true signal leaving out the small amplitude noisy signals.

Here we have investigated processing of signal pulse of varying qualities by bistable switches generated by a positive feedback loop either due to a mutual activation or a mutual inhibition between the two participating regulators. We varied three different pulse parameters, amplitude, duration and residual amplitude, to determine the effects of these parameters on the transition kinetics from one stable steady state to the other stable steady state for a population bistable switch. As a pulse of signal can lead to population inversion, we estimated the fraction of population that inverts to the other steady state, the fraction that is locked in the inverted state and the fraction that reverts to the original state. In addition, we quantified the time the bistable system takes to execute these events in order to understand the kinetics of pulse induced switching. Further, we correlated the durations of two consecutive events to determine how the history of previous event influences the future outcome. We compared the statistical properties of the various events between two bistable systems to determine the role of regulatory networks in dictating the chemical noise.

ACCEPTED

2. Results

We modeled bistable switches generated by two different mechanisms in which the required positive feedback loop was achieved either by mutual inhibition or by mutual activation between the two regulators. While the mutual activation creates a conventional positive feedback loop (PFL) motif, the mutual inhibition creates a double negative (DNFL) motif (Fig.1a-b). We used multisite phosphorylation of the target protein to generate ultrasensitive activation/inhibition of the protein that takes part in the positive feedback loop leading to bistable response (Kapuy et al., 2009; Salazar and Höfer, 2007). Multisite phosphorylation with threshold mechanism is known to generate ultrasensitive response with mass action rate laws of chemical reactions and has been used previously to model bistable switches in cell division cycle of *Saccharomyces cerevisiae* (Barik et al., 2010). In the model diagrams, the protein X possesses ten phosphorylation sites and its activation state is altered by phosphorylation catalyzed by the kinase, K. In the DNFL motif, the unphosphorylated state, X_0, is the active protein that catalyzes the degradation of the kinase and the kinase inactivates it by catalyzing the phosphorylation (**Fig.1a**). Therefore, the mutual antagonism between X_0 and K generates the DNFL motif in the network. In the PFL motif the terminally phosphorylated state, X_{10}, is the active protein that catalyzes the production of the kinase creating a PFL motif in the network (**Fig.1b**). The S is the phosphatase that catalyzes the dephosphorylation reactions and its level was controlled externally considering it as a parameter. We used mass action kinetics of the chemical reactions to model the dynamics of the chemical species in the network. The sole motivation of using mass action kinetics was to accurately capture the effects of fluctuations of molecular abundance in the dynamics of the system. It is crucial to note that, the well-established Gillespie's stochastic simulation algorithm faithfully captures the effects of intrinsic noise only for the mass action rate laws of chemical reactions (Gillespie, 1976). The dynamical equation for the kinase in the DNFL is given by

$$\frac{dN_K}{dt} = k_s - k_d N_K - k_a N_{X_0} N_K \tag{1}$$

The dynamical equation for the kinase in the PFL is given by

$$\frac{dN_K}{dt} = k_s + k_a N_{X_{10}} N_K - k_d N_K \tag{2}$$

The dynamical equations for the chemical species in the phosphorylation chain are given by

ACCEPTED

$$\frac{dN_{X_0}}{dt} = S \cdot N_{X_1} - k_p N_K N_{X_0} \quad (3)$$

$$\frac{dN_{X_j}}{dt} = S \cdot N_{X_{j+1}} + k_p N_K N_{X_{j-1}} - k_p N_K N_{X_j} - S \cdot N_{X_j} \quad \text{for } 2 \leq j \leq 9 \quad (4)$$

$$\frac{dN_{X_{10}}}{dt} = k_p N_K N_{X_9} - S \cdot N_{X_{10}} \quad (5)$$

In these equations N_j represents the molecular abundance of the chemical species j. The parameters k_s, k_d, k_a and k_p are the rate constants associated with synthesis, degradation, catalytic effects of X and K, respectively. The parameter values used in the calculations are listed in the table 1.

Table 1: List of parameters and their values.

Parameters	Model	
	DNFL	PFL
k_s	1.0	0.06
k_d	0.001	0.001
k_a	0.0002	0.01
k_p	0.005	0.01

The one-parameter bifurcation diagrams of the DNFL and PFL networks are presented in the **Fig.1c** and **Fig.1d**, respectively. In the bifurcation analysis, the phosphatase, S, was chosen as the bifurcation parameter. The system is bistable in the region between the two saddle-node bifurcation points. In both the models, the amount of kinase decreases with increasing phosphatase. In the DNFL network, with the increase of the phosphatase, the abundance of X_0 increases leading to decrease of the kinase. In the PFL network, however, the increased phosphatase decreases the availability of X_{10} leading to reduction of kinase production. For a fair comparison of pulse processing by the DNFL and PFL motifs, we parameterized these models such that a reasonably similar bifurcation diagrams can be obtained.

ACCEPTED

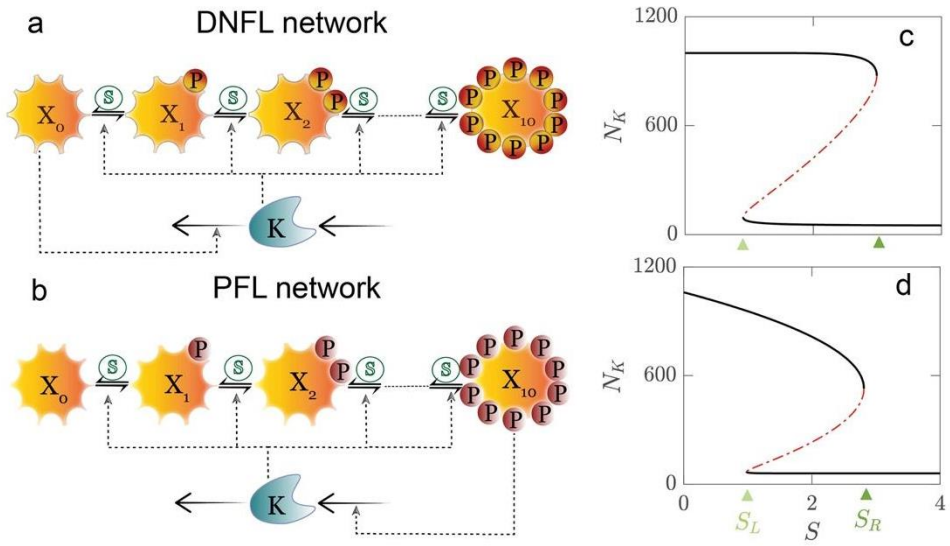

Fig.1: In the network diagrams of DNFL (a) and PFL (b) networks, the kinase, K, catalyzes the phosphorylation of the target protein X. In return, the active form of X catalyzes the degradation of the kinase in the DNFL network and catalyzes the production of K in the PFL network creating net positive feedback loops. The unphosphorylated (X_0) and terminally phosphorylated (X_{10}) forms are assumed to be the active forms of X in the DNFL and PFL networks, respectively. The solid and dashed lines represent chemical reactions and catalytic effects on the chemical reaction, respectively. The bistable one-parameter bifurcation diagrams of the DNFL (c) and PFL (d) are presented with the phosphatase (S) as the bifurcation parameter. The triangles indicate the signal values corresponding to the left (S_L) and right (S_R) saddle-node bifurcation points. The values of S_L and S_R, respectively, are 0.91 and 2.98 for the DNFL network and 0.98 and 2.82 for the PFL network.

We have investigated the fate of the system under a pulse of phosphatase in the face of inherent stochasticity of the system originating from the finite number of molecular species involved. In order to accurately estimate the stochasticity in the system we used Gillespie's stochastic simulation algorithm to simulate the chemical reactions in the model. In the computational experimental setup, we initialized the system at a very low phosphatase level ($S = 0.001$) and simulated for a sufficiently long time such that it reaches its steady state corresponding to the upper stable branch of the bifurcation diagram. The initial state of the system belonged to the monostable region of the bifurcation diagram with a high level of the kinase at $S = 0.001$ (before left saddle-node bifurcation point). A pulse of phosphatase of a certain amplitude (S_m) was applied for a particular duration (τ_d) and then the pulse amplitude was lowered to a residual or resting value (S_r) for the rest of the simulation (**Fig.2a**). We varied the pulse

amplitude, duration and resting pulse to determine the effects of these three parameters on the transition kinetics of the upper stable steady of the bistable systems. In the variation of pulse amplitude S_m, the lowest value was chosen to be the level of phosphatase corresponding to the right saddle-node bifurcation point (S_R) as beyond S_R the system is monostable with low expression of the kinase. While in the variation of resting pulse S_r, the minimum value was chosen to be the level of phosphatase corresponding to the left saddle-node bifurcation point (S_L) such that the system is bistable region with a possibility of locking either in low or high expression of the kinase. There are four different temporal outcomes possible due to the pulse of phosphatase: the system may not at all respond to the pulse (**Fig.2b**) or the system may transiently respond to the pulse by lowering the expression of the kinase (**Fig.2c**) or the system may invert to the other steady state either remaining there (**Fig.2d**) or switching back to the original state (**Fig.2e**). Therefore, in order to quantitatively estimate the fates of the bistable system under the pulse, we calculated the fraction of population that did not respond to the pulse (f_{nrs}), the fraction of population that responded transiently without reaching the lower steady state (f_{trn}), the fraction of population that flipped to the lower steady state (f_{inv}), the fraction of inverted population that switched back to the upper steady state (f_{swt}) and the fraction of inverted population that is locked in the lower steady state (f_{lck}). Furthermore, we computed the time scales associated with the various transitions as indicated in the schematic diagram (**Fig.2e**). We defined the inversion time (τ_{inv}) as the time the system takes to reach the lower steady state since the switching on of the pulse. The residence time (τ_{rsd}) and the switching time (τ_{swt}) were defined, respectively, as the duration that the system spends in the lower steady state before switching to the upper steady state and the time it takes to switch from the lower to the upper steady state. In addition, the inversion time was divided into an initial delay phase (τ_{dly}) and subsequent rapid response phase (τ_{rsp}).

ACCEPTED

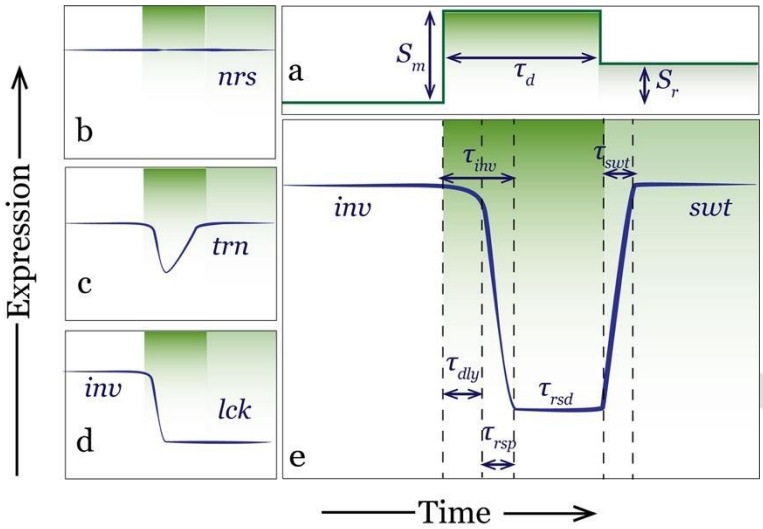

Fig.2: Schematic representations of the signal pulse (a) and various possible temporal outcomes of the kinase (b-e). The pulse dose (S_m), duration (τ_d) and resting dose (S_r) are the three parameters that characterize the pulse of phosphatase. The four possible temporal outcomes of the kinase are: (b) non-responding trajectory (*nrs*), (c) transient trajectory with reduced expression without reaching the lower steady state (*trn*), (d) inversion (inv) of the steady state with permanently locked in the lower steady state (*lck*) and (e) inversion and subsequent switching to the upper steady state (*swt*). The time scales associated with the inversion of steady state, residence in the lower steady state and switching into the upper steady state are represented, respectively, as τ_{inv}, τ_{rsd} and τ_{swt}. The inversion time is divided into an initial delay phase (τ_{dly}) and subsequent response phase (τ_{rsp}). The dark and light shaded regions indicate the pulse with maximum amplitude and pulse with resting amplitude, respectively.

We first present the dependence of the various population fractions on the pulse parameters. In **Fig.3a-b** the fraction of population that flips to the lower steady state is plotted as a function of pulse dose and duration for the DNFL and PFL motifs. The f_{inv} increases nonlinearly with increased pulse dose and duration indicating that the population inversion can be achieved by a pulse of phosphatase in which a strong pulse for a very short duration or a weak pulse for prolonged duration both can change the steady state of the bistable system. When the pulse duration is short, the bistable system requires a stronger pulse for the population inversion to occur and a small amplitude pulse can induce population inversion if the pulse duration was longer. The sharpness in the f_{inv} vs τ_d curves are more as compared to the sharpness in the f_{inv} vs ΔS_R suggesting that the criticality of pulse duration is more than the pulse amplitude. The sharp change in f_{inv} with τ_d suggests that a critical duration of pulse is required for population inversion, particularly in the PFL. Although the qualitative effect of pulse on the bistable

ACCEPTED

switch originated from the DNFL and PFL motifs are similar, however, PFL requires prolonged exposure of the pulse (large τ_d) as compared to the DNFL for population inversion. Particularly, even a transient pulse can induce significant population inversion in the DNFL motif, while the PFL network needs a pulse of prolonged duration. We calculated the pulse duration that is required to achieve 1% population inversion for both the systems across various pulse amplitudes. The decrease of this duration with increasing pulse dose suggests the complementary roles of pulse dose and duration (**Fig.3c**). Furthermore, the PFL needs a significantly large duration of pulse, as compared to the DNFL, to initiate the population inversion. In addition, the curved edge of the flat region indicates that a minimum dose and duration are required to cause a complete population inversion. In order to pinpoint the major player between the dose and duration, we calculated the area under the pulse required to obtain 99% population inversion (**Fig.3d**). The area signifies the integrated phosphatase signal that is exposed to the bistable system. The area as a function of the dose and duration indicate that the minimum pulse duration needed to cause 99% of population inversion is significantly higher in the PFL as compared to the DNFL. This suggests that PFL is less susceptible to the external signal as compared to the DNFL. Therefore, a transient signal (or noisy) signal may not lead to the change of the steady state in a PFL. Further, the decrease of the area with increasing dose indicates that the pulse dose has stronger effect in population inversion than the duration in flipping the state. We repeated these calculations with different values of resting pulse to establish that the population inversion dynamics in a bistable system is independent on the magnitude of the resting pulse (Supplementary Fig.S1).

ACCEPTED

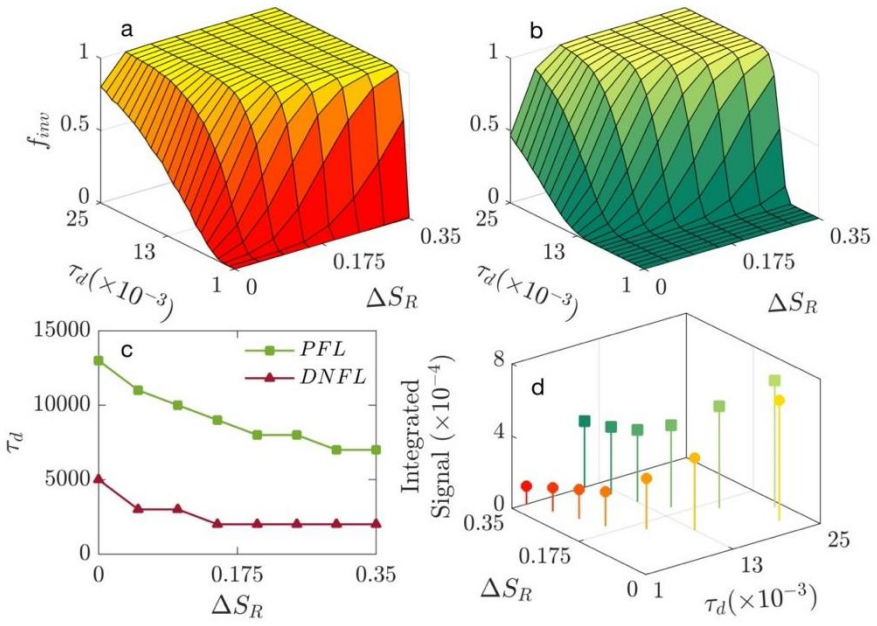

Fig.3: The fraction of population that flips into the lower steady state (f_{inv}) is plotted as a function pulse duration (τ_d) and pulse dose ($\Delta S_R = S_m - S_R$) for the DNFL (a) and PFL (b) networks. ΔS_R represents the pulse amplitude relative to the right saddle-node bifurcation point. In (c) The duration of pulse required to attain 1% population inversion is plotted as a function of ΔS_R. The integrated signal required for 99% population inversion is plotted as a function of τ_d and ΔS_R for the DNFL (circles) and PFL (squares) networks (d). The value of the resting pulse was the value of the signal corresponding to the left bifurcation point.

In order to study the transient nature of the bistable system under the pulse, we quantified the fraction of population that does not respond (f_{nrs}) and the fraction of population that responds transiently without reaching the lower steady state (f_{trn}). We found a stark contrast between the DNFL and PFL network in their transient dynamics. In the DNFL motif, f_{nrs} decreases with increasing dose and duration of the pulse (**Fig.4a**) and f_{trn} are quite low across various doses and duration of the pulse (**Fig.4b**). These indicate that the trajectories that responded to the pulse reached the lower steady state as the transient fractions are less across various doses and durations. Whereas in the PFL, f_{nrs} are nearly zero across all doses and durations suggesting that the entire population makes a response to the pulse irrespective of the pulse parameters (**Fig.4c**). The decrease of f_{trn} with increased pulse parameters in a dose dependent manner suggesting that after an initial transient response the trajectories flip to the lower steady state depending on the pulse parameters (**Fig.4d**). Therefore, the DNFL makes a single-step decision of flipping its steady state based on the quality of the pulse and the PFL makes this choice later

after an initial transient response to the pulse. Although a PFL motif is more susceptible to transient response, as compared to the DNFL, however PFL requires signal for prolonged duration for inverting the steady state indicating that PFL is less prone to perturbation due to the pulse. We verified that the initial responses of the system against the pulse are independent of resting pulse (Supplementary Fig.S2).

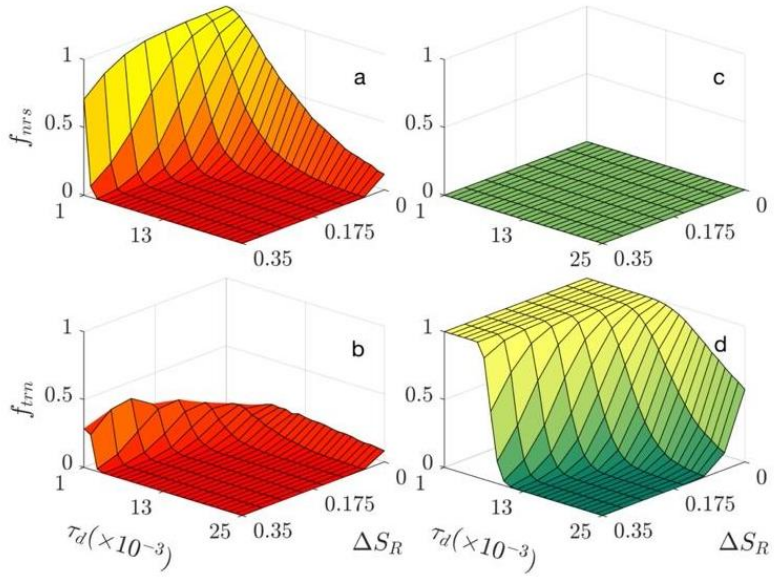

Fig.4: The fraction of non-responding, f_{nrs}, (top row) and transiently responding, f_{trn}, population (bottom row) are plotted as a function of τ_d and ΔS_R for the DNFL (left) and PFL (right) networks. The value of the resting pulse was the value of the signal corresponding to the left bifurcation point.

The time that the bistable system takes to switch from one state to another is an important aspect as it provides information about the kinetics of inversion in the dynamical system. The average time of flipping the steady state ($< \tau_{inv} >$), since the switching on of the pulse, are plotted as a function of pulse dose and duration for the two bistable switches (**Fig.5a-b**). The $< \tau_{inv} >$ decreases with the increasing pulse amplitude as the transition is facilitated by an intense pulse (left to right in Fig.5-b). At the low dose, the dependence of $< \tau_{inv} >$ on the pulse duration, however, is somewhat nonintuitive where $< \tau_{inv} >$ increases with τ_d for both the bistable systems (bottom to top in Fig.5-b). The increase of $< \tau_{inv} >$ implies that although a sustained weak signal may induce population inversion however, it comes at the cost of time. In order to determine the reason of this nonintuitive behavior, we looked at the trajectories under the pulse (**Fig.5g-h**). These trajectories indicate that the system does not respond immediately to the pulse in the DNFL network and after an initial delay the system rapidly transition to

the lower steady state (**Fig.5g**). On the contrary, in the case of PFL network, all trajectories respond immediately to the pulse by exhibiting a sluggish decrease of kinase level and after this initial phase the system rapidly jumps to the lower steady state (**Fig.5h**). Therefore, for better understanding, we partitioned the inversion time into an initial delay phase (τ_{dly}) and the subsequent rapid response phase (τ_{rsp}). In the case of DNFL, the average duration of the initial delay phase increases with increasing τ_d in the low dose regime (**Fig.5c**) and the average duration of the response phase is nearly independent of the dose and duration of the pulse (**Fig.5e**). Therefore, at low dose, the increase of $< \tau_{inv} >$ with τ_d is due to the increased average delay in the DNFL. The increase of delay is due to the fact that larger pulse duration allows more trajectories to flip their state at a later time and thereby prolonging the average time of response. It is important to note that, such phenomena happens when the magnitude of the dose is close to the right saddle-node bifurcation point ($\Delta S_R \sim 0$). Therefore, it suggests that the delay in making a decision of flipping is most likely due to the critical slowing down of the system near the bifurcation point. At a large dose the system remains far away ($\Delta S_R \gg 0$) from the bifurcation point and therefore critical slowing down related delay does not occur. Consequently, the system responds faster and $< \tau_{rsp} >$ becomes independent of the pulse duration. The dose and duration independence of $< \tau_{rsp} >$ suggests that once the decision of transition is made the system self-propels itself into the lower steady state in a pulse independent manner. Therefore the increase of the average transition time with pulse duration is due to the increased delay in initial response in the DNFL system. In the case of PFL, the dynamics of the system is quite different than that of the DNFL motif. Here $< \tau_{dly} >$ is nearly independent of τ_d (**Fig.5d**), whereas $< \tau_{rsp} >$ increases with τ_d at the low pulse dose (**Fig.5f)**. Therefore, the effect of the critical slowing down is manifested exclusively in the second phase of the switching dynamics in the PFL motif. We found that these durations do not depend on the magnitude of the resting pulse (Supplementary Fig.S3).

ACCEPTED

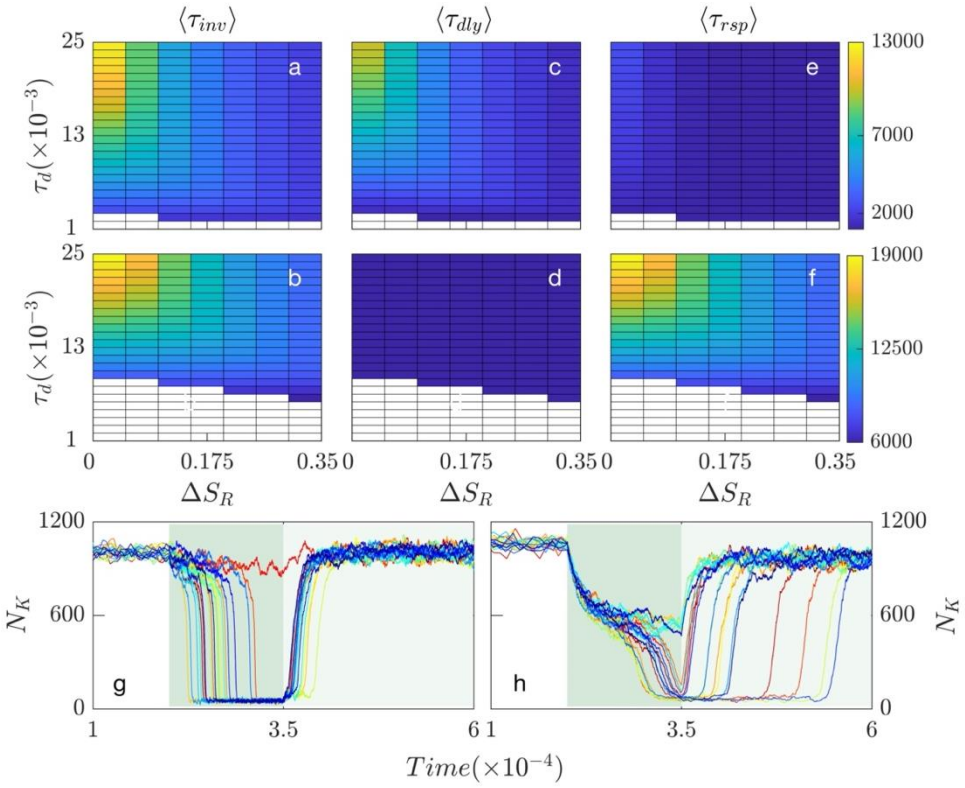

Fig.5: The surface plots of average inversion time ($\langle\tau_{inv}\rangle$), average initial delay time ($\langle\tau_{dly}\rangle$) and average response time ($\langle\tau_{rsp}\rangle$) are presented as a function of τ_d and ΔS_R for the DNFL (top row) and PFL (middle row) networks (a-f). The pulse induced temporal dynamics of the kinase are shown for the DNFL (g) and PFL (h) networks. The dark and light shaded regions indicate the pulse on state with maximum and resting amplitudes, respectively. The value of the resting pulse was the value of the signal corresponding to the left bifurcation point.

The pulse of phosphatase forces the system to flip its steady state from the upper to the lower steady state. However, removal of the signal pulse may lead to returning of the system to the original state. Thus, we determined next the fate of the flipped state upon removal of the pulse while maintaining a residual signal level. We calculated the fraction of cells that returned to the upper steady state (f_{swt}) as a function of various parameters of the pulse. f_{swt} critically depends on the magnitude of the resting pulse, S_r or ΔS_L. At low resting pulse, the entire population returns back to the upper steady state irrespective of the duration (**Fig.6a-b**) and amplitude (Supplementary Fig.S4) of the pulse for both the bistable systems. However, with the increase of the resting pulse (large ΔS_L) the fraction of population returning decreases in a nonlinear manner and consequently the fraction of locked population in the lower steady state increases in a complementary manner (Supplementary Fig.S5). Therefore, although a

pulse of signal may induce flipping of the state however to maintain the flipped state a residual signal is necessary. A comparison of f_{swt} vs. ΔS_L curves between DNFL and PFL networks revealed that f_{swt} decreases sharply with the resting pulse in DNFL network as compared to the PFL network (Supplementary Fig.S6). Consequently, at a particular resting pulse, relatively a larger fraction of population switches back to the upper steady state in PFL network as compared to DNFL network. The bifurcation diagram provides a clue to this difference between the DNFL and PFL system. Although the at low ΔS_L the system remains within the bistable region, however in the PFL network the close proximity of the unstable branch with a small basin of attraction allowed the system to make a chemical noise assisted transition to the upper steady state that has a large basin of attraction near the left bifurcation point. Consistent with the population results, the increased resting pulse leads to elevated average residence time ($< \tau_{rsd} >$) of the lower steady state (**Fig.6c-d**). A moderate increase of $< \tau_{rsd} >$ is noted with the increased τ_D as longer pulse allows the system to spend longer in the lower steady state. Supplementary Fig.S4 confirms that the pulse dose does not play any role in the residence and return dynamics of the system. The average switching time ($< \tau_{swt} >$) from the lower to the upper steady state increases marginally with the resting pulse, however $< \tau_{swt} >$ is mostly independent of the dose and the duration of the pulse (**Fig.6e-f**).

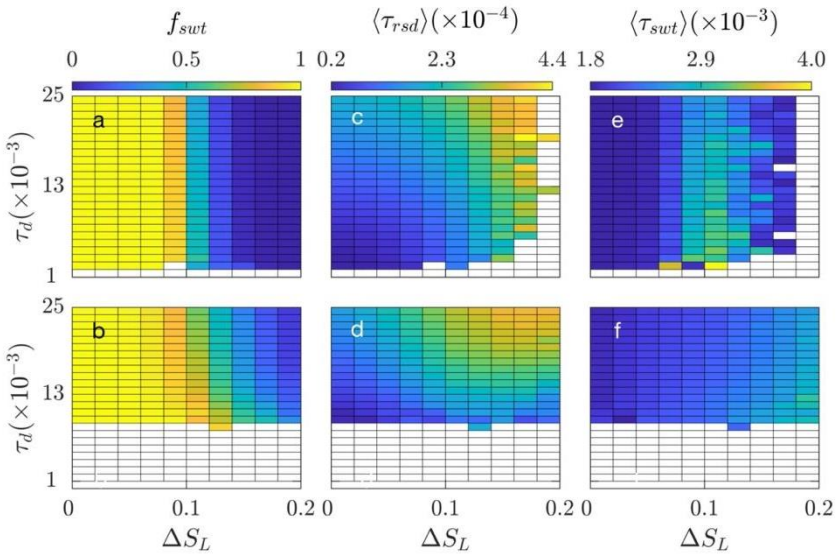

Fig.6: The fraction of the population that switches back to the upper steady state (f_{swt}), the average residence time in the lower steady state ($\langle\tau_{rsd}\rangle$) and the average switching time ($\langle\tau_{swt}\rangle$) are plotted as a function of pulse duration and resting pulse ($\Delta S_L = S_m - S_L$) for the DNFL (top row) and PFL (bottom row)

ACCEPTED

networks. ΔS_L represents the resting pulse over and above the signal value corresponding to the left saddle node bifurcation point. The value of the ΔS_R was 0.1.

Previous studies have highlighted that regulatory networks play a crucial role in attenuating the chemical noise biochemical reaction networks (Dey and Barik, 2017; Hornung and Barkai, 2008; Raj and van Oudenaarden, 2008). Therefore, in order to understand the role of feedback loops in regulating the chemical noise, we compared the statistical properties of inversion and switching time between the DNFL and PFL networks (**Fig.7a-d**). The comparison of average duration of inversion and switching time show that the bistability from PFL motif takes more time to make a transition from one steady state to the other steady state (**Fig.7a-b**). Furthermore, the noise, quantified as the coefficient of variation (CV), in these two times are significantly less in the case of PFL as compared to the DNFL network (**Fig.7c-d**). It is worth noting that the noise in the inversion time increases with τ_D for both the networks. This is due to increased relative available time ($= (\tau_D - < \tau_{inv} >)/\tau_D$) for the system to respond against the pulse (**Fig.7e**). The relative available time measures the amount of extra time available, over and above the average inversion time, by the system to respond to the pulse. Large relative available duration would accommodate a greater number of late responders contributing to increased variability. As the switching dynamics is autonomous in nature therefore the CV and average of τ_{swt} are independent of τ_D. These two results suggest that the bistable switch originating from a PFL is less susceptible to the external pulse as compared to the bistable switch from a DNFL. Therefore, a PFL motif will be less prone to make a stochastic transition from one state to the other due to external noisy signal and consequently a PFL will be more robust to external perturbations of noisy signal by efficiently filtering out the spurious signals. Consequently, the population heterogeneity of a bistable switch originated from mutual inhibition will be more as compared to a bistable switch from mutual activation. By repeating these calculations for different values of pulse amplitudes, we confirmed that greater robustness of PFL persists across various pulse amplitudes (Supplementary Fig.S7).

ACCEPTED

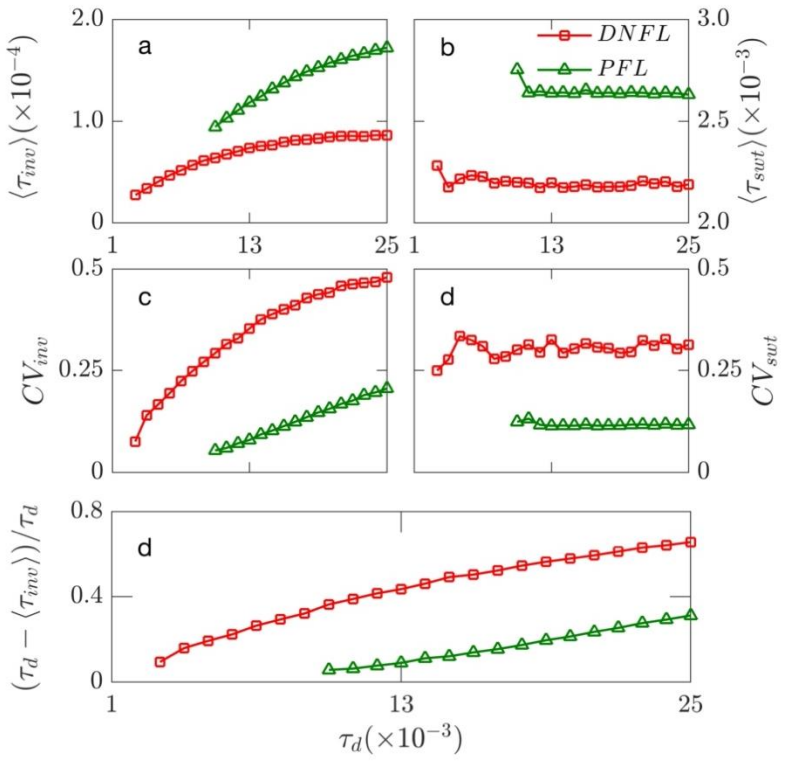

Fig.7: The comparison of statistical properties of inversion and switching times between the DNFL and PFL networks (a-d). The comparison of relative available time vs. τ_d between the DNFL and PFL networks. The values of the pulse dose and resting pulse were $\Delta S_R = 0$ and $\Delta S_L = 0$.

In the **Fig.8a-c** the correlation between the inversion time and the residence time of individual trajectories are plotted for the DNFL motif to find out whether the history of the system influences the future outcome in the dynamics. The negative correlation between these two events implies that the trajectory that made an early transition to the lower steady state stayed for a longer duration there. Furthermore, a larger value of the correlation coefficient implies that these two events are tightly controlled by the external pulse or in other words the temporal behavior of the system is more predictable in nature. For the DNFL network, the correlation decreases with increased pulse duration (**Fig.8a**) implying that exposure of small amplitude signal for a prolonged duration may lead to delayed inversion of the steady state, however such inversion would be temporary. Therefore, the dynamics of the system is tightly regulated (more predictable or correlative) when the state inversion is induced by a sustained signal. On the contrary, a shorter pulse results in increased variability of τ_{rsd} and consequently the correlation between the two events becomes less making the future outcome more unpredictable relative to the past event. Increased resting pulse (**Fig.8b**) and pulse dose (**Fig.8c**) lead to

poor correlations between these two times. However, the origins of reduced correlations due to higher dose and resting pulse are not same. The dose controls the population inversion dynamics (or τ_{inv}) and therefore larger dose skews the population towards smaller $< \tau_{inv} >$, without affecting the switching dynamics, leading to decoherence of the two events. At a smaller resting pulse, the temporal dynamics of the system correlate well with the temporal profile of the pulse and consequently, the correlation coefficient between τ_{inv} and τ_{rsd} is large at a smaller resting pulse. A larger resting pulse forces the system to be at the lower steady state with larger $< \tau_{rsd} >$ thus the temporal correlation between the pulse and dynamics of the system is lost leading to the decreased correlation coefficient. In the case of PFL, the qualitative effects of pulse parameters on the correlation are similar to the DNFL, however here the correlations are generally poor as compared to DNFL across various pulse parameters (Fig.8d and Supplementary Fig.S8).

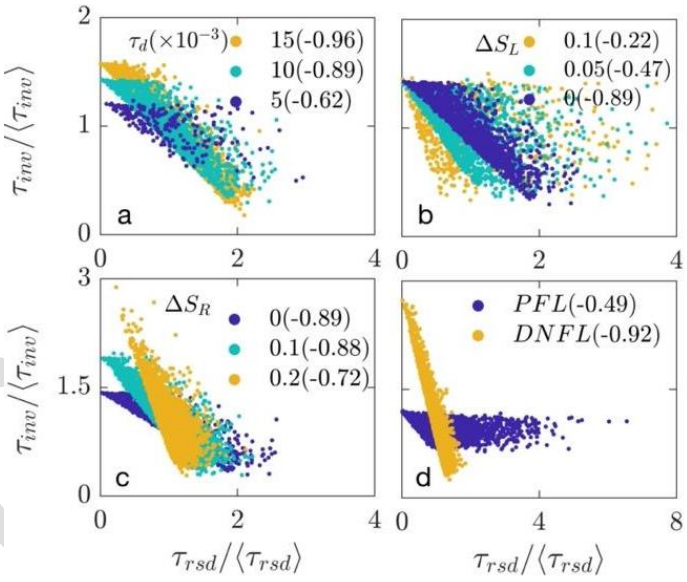

Fig.8: The correlation between the mean-normalized τ_{inv} and τ_{rsd} are plotted for the indicated values of τ_d (a), ΔS_L (b) and ΔS_R (c) for the DNFL network. The values of correlation coefficients are indicated within the parenthesis inside each plot. In (d) the correlation between these two times are compared for the DNFL and PFL networks. The pulse parameters used were: $\Delta S_R = 0$ and $\Delta S_L = 0$ in (a); $\tau_d = 1 \times 10^4$ and $\Delta S_R = 0$ in (b), $\tau_d = 1 \times 10^4$ and $\Delta S_L = 0$ in (c) and $\tau_d = 1.5 \times 10^4$, $\Delta S_R = 0.1$ and $\Delta S_L = 0$ in (d).

We extended these calculations to networks with two fused positive feedback loops centered around the kinase, K. In the two-loop networks, another protein regulator, Y, was introduced with 10 phosphorylation sites and possessing a similar causal relationship with the kinase K. **Fig.9a** and **Fig.9b**

represent the network diagrams consisting of the two fused DNFLs and two fused PFLs, respectively. Different forms of Y will have similar dynamical equations as listed in the case of single positive feedback loop (Eq.3-4). In the DNFL network, the equation for the kinase consists of another degradation term due to the catalytic effect of Y_0 on the kinase. Similarly, the dynamical equation for the kinase consists of another synthesis term due to Y_{10} in the PFL network. Here the value of k_a was reduced by a factor of 2, as compared to single loop case, in order to obtain the identical bifurcation diagrams as in the case of single positive feedback loop. All other parameters were the same as in the case of single loop. In the two loops case, the fractions of population that flip to the other steady state are slightly higher across various doses and durations of the pulse (**Fig.9c-d**). Therefore, pulse induced transitions to the other steady state are facilitated by the additional positive feedback loop.

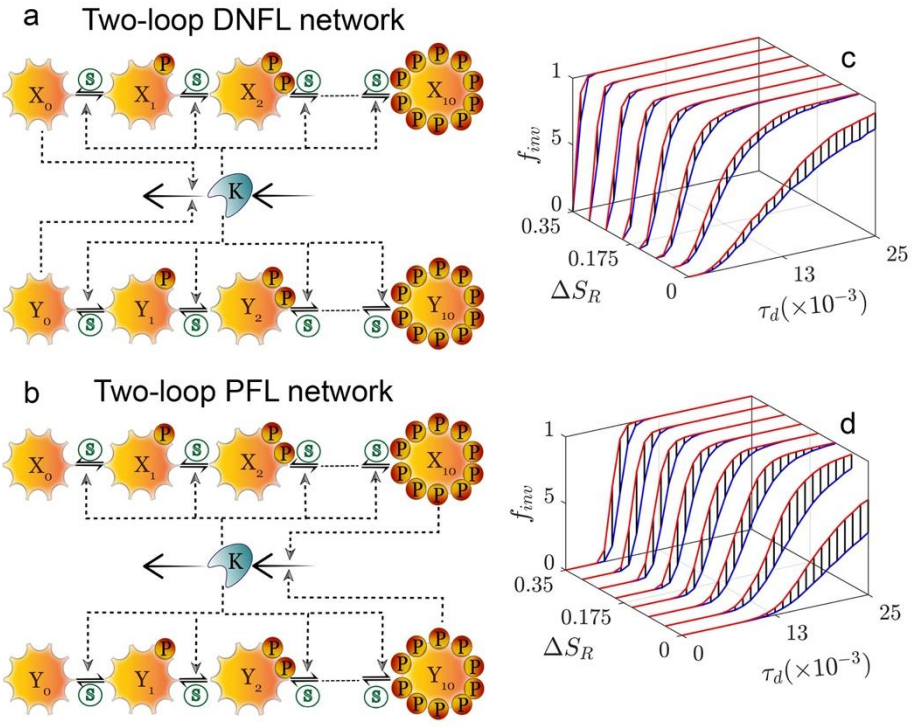

Fig.9: The network diagrams of two fused DNFLs (a) and two fused PFLs (b). Here, one more positive feedback loop was introduced either by mutual inhibition (a) or by mutual activation (b) between K and Y. Analogous to X, the phosphorylation and dephosphorylations of Y are catalyzed by the kinase, K, and the phosphatase, S, respectively. The plots of f_{inv} as a function of pulse dose (ΔS_R) and duration (τ_d) are compared between one-loop (blue lines) and two-loop (red lines) DNFL (c) and PFL (d) networks. The vertical black lines indicate the difference between the two lines. The value of the resting pulse was the value of the signal corresponding to the left bifurcation point.

3. Conclusions

Processing various external and internal signals are key to living organisms for the proper functioning of physiology at the cellular and organismal levels. Cells often receive signals in discrete manner with varying amplitudes, durations and intervals. In order to understand the processing of transient signal by a regulatory motif, we investigated the fate of a bistable switch generated either by mutual activation (PFL) or by mutual inhibition (DNFL) between two regulators.

We find that a pulse of signal can induce population inversion by driving the bistable system into the other stable steady state and such inversion can be achieved either by a strong transient signal or by a prolonged weak signal indicating that the dose or duration can be compensated by each other. Between the pulse amplitude and duration, amplitude imparts a stronger effect on the inversion dynamics in bistable switches. The pulse amplitude facilitates population inversion by reducing the average inversion time irrespective of the nature of the bistable network. Whereas the pulse duration facilitates inversion by accommodating more numbers of late responders that take a longer time to switch to other steady state. As a consequence, in the weak dose regime, the average inversion time increases significantly with the pulse duration. This also confirms that the critical slowing down of the trajectories strongly influence the dynamics when the signal dose is close to the saddle-node bifurcation point. We find critical differences in processing of pulse by a mutual activation and a mutual inhibition loop. Irrespective of pulse parameters, a bistable switch originating from mutual activation motif makes an immediate transient response to the pulse and the average duration of this initial response is independent of the pulse duration. After this initial response, the system flips to the other steady state with an average duration that depends strongly on the pulse duration. On the contrary, the mutual inhibition motif does not exhibit a transient initial response. After a pulse duration dependent initial delay, it rapidly self-propels into the lower steady state. Here the average duration of the initial delay depends strongly on the pulse duration but the second phase is independent of the pulse duration.

Although the population inversion is independent of the resting pulse, however, the fraction of population locked in the flipped state and the average residence time in the flipped state strongly depends on the residual signal in the form of resting pulse. Whereas, the pulse amplitude and duration do not have much role in dictating the dynamics of the flipped state. Therefore, a pulse of signal may lead to inversion of steady state, however to maintain the inverted state the system requires a residual signal. The average duration of inversion and switching times associated with the upper and lower steady states of bistable system are higher in the mutual activation network as compared to the mutual

ACCEPTED

inhibition network. Furthermore, the variabilities in these two times are significantly smaller in the mutual activation network as compared to the mutual inhibition network. In addition, mutual activation requires a pulse of significantly prolonged duration as compared to mutual inhibition loop in order to cause population inversion. These three results indicate that the mutual activation network is less susceptible to responding to the transient signal and therefore a bistable system originating from mutual activation would be a better topology to filter noisy external signals. These conclusions are consistent with previous finding that mutual activation networks are better topology in attenuating chemical noise in the context of sustained signaling (Hornung and Barkai, 2008).

The correlations between the inversion time and residence time indicate that the pulse induced inversion and subsequent revival to the original state are tightly regulated by weak pulse of prolonged duration. This suggests that the system behaves in a deterministic or predictable fashion when the inversion of steady state is caused by signal of longer duration. Thus, although a short intense pulse may induce flipping of steady state efficiently however the behavior of the subsequent events becomes less predictable. Therefore, it features that the noise in the system can also be controlled by an external signal.

The pulse of signal can be used in controlling the ratio of population for a system having two possible cellular fates (Menn et al., 2019). The mixed population in the bistable system can either be achieved by noise induced transition leading to stochastic switching of one state to the other in the bistable regime or it can be achieved by the pulse of signal where the signal amplitude remains outside the bistable regime. In this study, we systematically investigated the effect of signal pulse with amplitude outside the bistable regime and determined the various populations and the associated time scales. Our work reveals the fate of the system under the pulse of various qualities and underscores the key differences by which PFL and DNFL motif process the pulse.

4. Methods

The one-parameter bifurcation analyses of the models were performed by the software tool XPP-AUT. The stochastic simulations of the models were carried out by converting the model equations into the corresponding mass-action chemical reactions and simulating those chemical reactions using the Gillespie's stochastic simulation algorithm. The system was initialized at a very low value of the phosphatase (S=0.001) and simulated for sufficiently long time so that the system reaches its steady state

ACCEPTED

corresponding to the upper steady state of the bifurcation diagram. A pulse of the phosphatase was initiated and the trajectory of the kinase was monitored to estimate the fractions of the various populations and the associated time scales by triggering flags at different values of the kinase during its time course. Once the trajectory reaches a threshold value of 100, we count the trajectory as flipped trajectory and the time it takes to reach this value since the switching on of the pulse is the τ_{inv}. The trajectory with unaltered expression and with transiently lowered expression without reaching 100, was labeled as non-responder and transiently responder, respectively. To estimate the response delay (τ_{dly}), we used threshold values of 800 and 600, respectively, for DNFL and PFL networks. The response time (τ_{rsp}) was calculated by subtracting τ_{dly} from τ_{inv}. The residence time in the lower steady state (τ_{rsd}) was estimated by calculating the time the system takes to reach a threshold value of 150, after removal of the pulse, since reaching the lower steady state. Thereafter, the time taken to switch back to its upper steady state (τ_{swt}) was estimated when the system reached a threshold value of 850 and the trajectory was labelled as switched.

Author Contribution

S.D. and D.B. designed and performed research; A.D. and D.B. analyzed data; A.D. and D.B. wrote and revised the manuscript; D.B. acquired funding and supervised the project.

Acknowledgement

The work was supported by the MATRICS (grant no. MTR/2019/000935) research grant from the Science and Engineering Research Board, Department of Science and Technology (India) to DB. SD acknowledges fellowship from INSPIRE program of Department of Science and Technology, India.

ACCEPTED

References

Ajo-Franklin, C. M., Drubin, D. A., Eskin, J. A., Gee, E. P. S., Landgraf, D., Phillips, I., Silver, P. A., 2007. Rational design of memory in eukaryotic cells. Genes & Development 21, 2271-2276, doi:10.1101/gad.1586107.

Albeck, John G., Mills, Gordon B., Brugge, Joan S., 2013. Frequency-Modulated Pulses of ERK Activity Transmit Quantitative Proliferation Signals. Molecular Cell 49, 249-261, doi:https://doi.org/10.1016/j.molcel.2012.11.002.

Bagci, E. Z., Vodovotz, Y., Billiar, T. R., Ermentrout, G. B., Bahar, I., 2006. Bistability in Apoptosis: Roles of Bax, Bcl-2, and Mitochondrial Permeability Transition Pores. Biophysical Journal 90, 1546-1559, doi:http://dx.doi.org/10.1529/biophysj.105.068122.

Barik, D., Ball, D. A., Peccoud, J., Tyson, J. J., 2016. A Stochastic Model of the Yeast Cell Cycle Reveals Roles for Feedback Regulation in Limiting Cellular Variability. PLOS Computational Biology 12, e1005230, doi:10.1371/journal.pcbi.1005230.

Barik, D., Baumann, W. T., Paul, M. R., Novak, B., Tyson, J. J., 2010. A model of yeast cell cycle regulation based on multisite phosphorylation. Molecular Systems Biology 6.

Becker-Weimann, S., Wolf, J., Herzel, H., Kramer, A., 2004. Modeling Feedback Loops of the Mammalian Circadian Oscillator. Biophysical Journal 87, 3023-3034, doi:https://doi.org/10.1529/biophysj.104.040824.

Chang, D.-E., Leung, S., Atkinson, M. R., Reifler, A., Forger, D., Ninfa, A. J., 2010. Building biological memory by linking positive feedback loops. Proceedings of the National Academy of Sciences 107, 175-180, doi:10.1073/pnas.0908314107.

Chen, K. C., Calzone, L., Csikasz-Nagy, A., Cross, F. R., Novak, B., Tyson, J. J., 2004. Integrative Analysis of Cell Cycle Control in Budding Yeast. Molecular Biology of the Cell 15, 3841-3862, doi:10.1091/mbc.e03-11-0794.

Dalal, Chiraj K., Cai, L., Lin, Y., Rahbar, K., Elowitz, Michael B., 2014. Pulsatile Dynamics in the Yeast Proteome. Current Biology 24, 2189-2194, doi:https://doi.org/10.1016/j.cub.2014.07.076.

de la Cova, C., Townley, R., Regot, S., Greenwald, I., 2017. A Real-Time Biosensor for ERK Activity Reveals Signaling Dynamics during C. elegans Cell Fate Specification. Developmental Cell 42, 542-553.e4, doi:https://doi.org/10.1016/j.devcel.2017.07.014.

Dey, A., Barik, D., 2017. Parallel arrangements of positive feedback loops limit cell-to-cell variability in differentiation. PLOS ONE 12, e0188623, doi:10.1371/journal.pone.0188623.

Domingo-Sananes, M. R., Szöőr, B., Ferguson, M. A. J., Urbaniak, M. D., Matthews, K. R., 2015. Molecular control of irreversible bistability during trypanosome developmental commitment. The Journal of Cell Biology 211, 455-468, doi:10.1083/jcb.201506114.

Doncic, A., Atay, O., Valk, E., Grande, A., Bush, A., Vasen, G., Colman-Lerner, A., Loog, M., Skotheim, Jan M., 2015. Compartmentalization of a Bistable Switch Enables Memory to Cross a Feedback-Driven Transition. Cell 160, 1182-1195, doi:https://doi.org/10.1016/j.cell.2015.02.032.

Ferrell, J. E., 2016. Perfect and Near-Perfect Adaptation in Cell Signaling. Cell Systems 2, 62-67, doi:https://doi.org/10.1016/j.cels.2016.02.006.

Ferrell Jr, J. E., 2002. Self-perpetuating states in signal transduction: positive feedback, double-negative feedback and bistability. Current Opinion in Cell Biology 14, 140-148, doi:http://dx.doi.org/10.1016/S0955-0674(02)00314-9.

Gao, Z., Chen, S., Qin, S., Tang, C., 2018. Network Motifs Capable of Decoding Transcription Factor Dynamics. Scientific Reports 8, 3594, doi:10.1038/s41598-018-21945-2.

Gillespie, D. T., 1976. A general method for numerically simulating the stochastic time evolution of coupled chemical reactions. J. Comput. Phys. 22, 403-434.

ACCEPTED

Gonze, D., 2011. Modeling circadian clocks: From equations to oscillations. Central European Journal of Biology 6, 699, doi:10.2478/s11535-011-0061-5.
Hansen, A. S., O'Shea, E. K., 2016. Encoding four gene expression programs in the activation dynamics of a single transcription factor. Current Biology 26, R269-R271, doi:https://doi.org/10.1016/j.cub.2016.02.058.
Harton, M. D., Koh, W. S., Bunker, A. D., Singh, A., Batchelor, E., 2019. p53 pulse modulation differentially regulates target gene promoters to regulate cell fate decisions. Molecular Systems Biology 15, e8685, doi:https://doi.org/10.15252/msb.20188685.
Hayot, F., Jayaprakash, C., 2006. NF-κB oscillations and cell-to-cell variability. Journal of Theoretical Biology 240, 583-591, doi:https://doi.org/10.1016/j.jtbi.2005.10.018.
Hoffmann, A., Levchenko, A., Scott Martin, L., Baltimore, D., 2002. The IκB-NF-κB Signaling Module: Temporal Control and Selective Gene Activation. Science 298, 1241-1245, doi:10.1126/science.1071914.
Hornung, G., Barkai, N., 2008. Noise Propagation and Signaling Sensitivity in Biological Networks: A Role for Positive Feedback. PLOS Computational Biology 4, e8, doi:10.1371/journal.pcbi.0040008.
Imayoshi, I., Isomura, A., Harima, Y., Kawaguchi, K., Kori, H., Miyachi, H., Fujiwara, T., Ishidate, F., Kageyama, R., 2013. Oscillatory Control of Factors Determining Multipotency and Fate in Mouse Neural Progenitors. Science 342, 1203-1208, doi:doi:10.1126/science.1242366.
Kapuy, O., Barik, D., Domingo Sananes, M. R., Tyson, J. J., Novak, B., 2009. Bistability by multiple phosphorylation of regulatory proteins. Prog. Biophys. Mol. Biol. 100, 47-56.
Kholodenko, B. N., 2006. Cell-signalling dynamics in time and space. Nature Reviews Molecular Cell Biology 7, 165, doi:10.1038/nrm1838

https://www.nature.com/articles/nrm1838#supplementary-information.
Kim, J. K., Forger, D. B., 2012. A mechanism for robust circadian timekeeping via stoichiometric balance. Molecular Systems Biology 8, 630, doi:https://doi.org/10.1038/msb.2012.62.
Lane, K., Van Valen, D., DeFelice, M. M., Macklin, D. N., Kudo, T., Jaimovich, A., Carr, A., Meyer, T., Pe'er, D., Boutet, S. C., Covert, M. W., 2017. Measuring Signaling and RNA-Seq in the Same Cell Links Gene Expression to Dynamic Patterns of NF-κB Activation. Cell Systems 4, 458-469.e5, doi:https://doi.org/10.1016/j.cels.2017.03.010.
Leloup, J.-C., Goldbeter, A., 2003. Toward a detailed computational model for the mammalian circadian clock. Proceedings of the National Academy of Sciences 100, 7051-7056, doi:10.1073/pnas.1132112100.
Lormeau, C., Rudolf, F., Stelling, J., 2021. A rationally engineered decoder of transient intracellular signals. Nature Communications 12, 1886, doi:10.1038/s41467-021-22190-4.
Ma, W., Trusina, A., El-Samad, H., Lim, W. A., Tang, C., 2009. Defining Network Topologies that Can Achieve Biochemical Adaptation. Cell 138, 760-773, doi:https://doi.org/10.1016/j.cell.2009.06.013.
Mangan, S., Alon, U., 2003. Structure and function of the feed-forward loop network motif. Proceedings of the National Academy of Sciences 100, 11980-11985, doi:10.1073/pnas.2133841100.
Martinez-Corral, R., Raimundez, E., Lin, Y., Elowitz, M. B., Garcia-Ojalvo, J., 2018. Self-Amplifying Pulsatile Protein Dynamics without Positive Feedback. Cell Systems 7, 453-462.e1, doi:https://doi.org/10.1016/j.cels.2018.08.012.
Menn, D., Sochor, P., Goetz, H., Tian, X.-J., Wang, X., 2019. Intracellular Noise Level Determines Ratio Control Strategy Confined by Speed–Accuracy Trade-off. ACS Synthetic Biology 8, 1352-1360, doi:10.1021/acssynbio.9b00030.

ACCEPTED

Ochi, S., Imaizumi, Y., Shimojo, H., Miyachi, H., Kageyama, R., 2020. Oscillatory expression of Hes1 regulates cell proliferation and neuronal differentiation in the embryonic brain. Development 147, doi:10.1242/dev.182204.

Pomerening, J. R., Sontag, E. D., Ferrell Jr, J. E., 2003. Building a cell cycle oscillator: hysteresis and bistability in the activation of Cdc2. Nature Cell Biology 5, 346, doi:10.1038/ncb954

https://www.nature.com/articles/ncb954#supplementary-information.

Purvis, Jeremy E., Lahav, G., 2013. Encoding and Decoding Cellular Information through Signaling Dynamics. Cell 152, 945-956, doi:https://doi.org/10.1016/j.cell.2013.02.005.

Purvis, J. E., Karhohs, K. W., Mock, C., Batchelor, E., Loewer, A., Lahav, G., 2012. p53 Dynamics Control Cell Fate. Science 336, 1440-1444, doi:doi:10.1126/science.1218351.

Raj, A., van Oudenaarden, A., 2008. Nature, Nurture, or Chance: Stochastic Gene Expression and Its Consequences. Cell 135, 216-226, doi:10.1016/j.cell.2008.09.050.

Salazar, C., Höfer, T., 2007. Versatile regulation of multisite protein phosphorylation by the order of phosphate processing and protein–protein interactions. The FEBS Journal 274, 1046-1061, doi:https://doi.org/10.1111/j.1742-4658.2007.05653.x.

Sha, W., Moore, J., Chen, K., Lassaletta, A. D., Yi, C.-S., Tyson, J. J., Sible, J. C., 2003. Hysteresis drives cell-cycle transitions in Xenopus laevis egg extracts. Proceedings of the National Academy of Sciences 100, 975-980, doi:10.1073/pnas.0235349100.

Spencer, Sabrina L., Sorger, Peter K., 2011. Measuring and Modeling Apoptosis in Single Cells. Cell 144, 926-939, doi:https://doi.org/10.1016/j.cell.2011.03.002.

Tyson, J. J., Novák, B., 2010. Functional Motifs in Biochemical Reaction Networks. Annual Review of Physical Chemistry 61, 219-240, doi:doi:10.1146/annurev.physchem.012809.103457.

Tyson, J. J., Novak, B., 2020. A Dynamical Paradigm for Molecular Cell Biology. Trends in Cell Biology 30, 504-515, doi:https://doi.org/10.1016/j.tcb.2020.04.002.

Tyson, J. J., Chen, K. C., Novak, B., 2003. Sniffers, buzzers, toggles and blinkers: dynamics of regulatory and signaling pathways in the cell. Current Opinion in Cell Biology 15, 221-231, doi:http://dx.doi.org/10.1016/S0955-0674(03)00017-6.

Ueda, H. R., Hagiwara, M., Kitano, H., 2001. Robust Oscillations within the Interlocked Feedback Model of Drosophila Circadian Rhythm. Journal of Theoretical Biology 210, 401-406, doi:https://doi.org/10.1006/jtbi.2000.2226.

Wang, L., Walker, B. L., Iannaccone, S., Bhatt, D., Kennedy, P. J., Tse, W. T., 2009. Bistable switches control memory and plasticity in cellular differentiation. Proceedings of the National Academy of Sciences 106, 6638-6643.

Yao, G., Lee, T. J., Mori, S., Nevins, J. R., You, L., 2008. A bistable Rb-E2F switch underlies the restriction point. Nat Cell Biol 10, 476-482, doi:http://www.nature.com/ncb/journal/v10/n4/suppinfo/ncb1711_S1.html.

Zambrano, S., De Toma, I., Piffer, A., Bianchi, M. E., Agresti, A., 2016. NF-κB oscillations translate into functionally related patterns of gene expression. eLife 5, e09100, doi:10.7554/eLife.09100.

Zhang, C., Tsoi, R., Wu, F., You, L., 2016. Processing Oscillatory Signals by Incoherent Feedforward Loops. PLOS Computational Biology 12, e1005101, doi:10.1371/journal.pcbi.1005101.

Zhang, J., Tian, X.-J., Zhang, H., Teng, Y., Li, R., Bai, F., Elankumaran, S., Xing, J., 2014. TGF-β–induced epithelial-to-mesenchymal transition proceeds through stepwise activation of multiple feedback loops. Science Signaling 7, ra91-ra91, doi:10.1126/scisignal.2005304.

NOT PEER REVIEWED

Supplementary figures to

Pulsatile signaling of bistable switches reveal the distinct nature of pulse processing by mutual activation and mutual inhibition loop

Soutrick Das and Debashis Barik*

School of Chemistry, University of Hyderabad, Central University P.O., Hyderabad, 500046, Telangana, India

*Corresponding author, E-mail: dbariksc@uohyd.ac.in

ACCEPTED

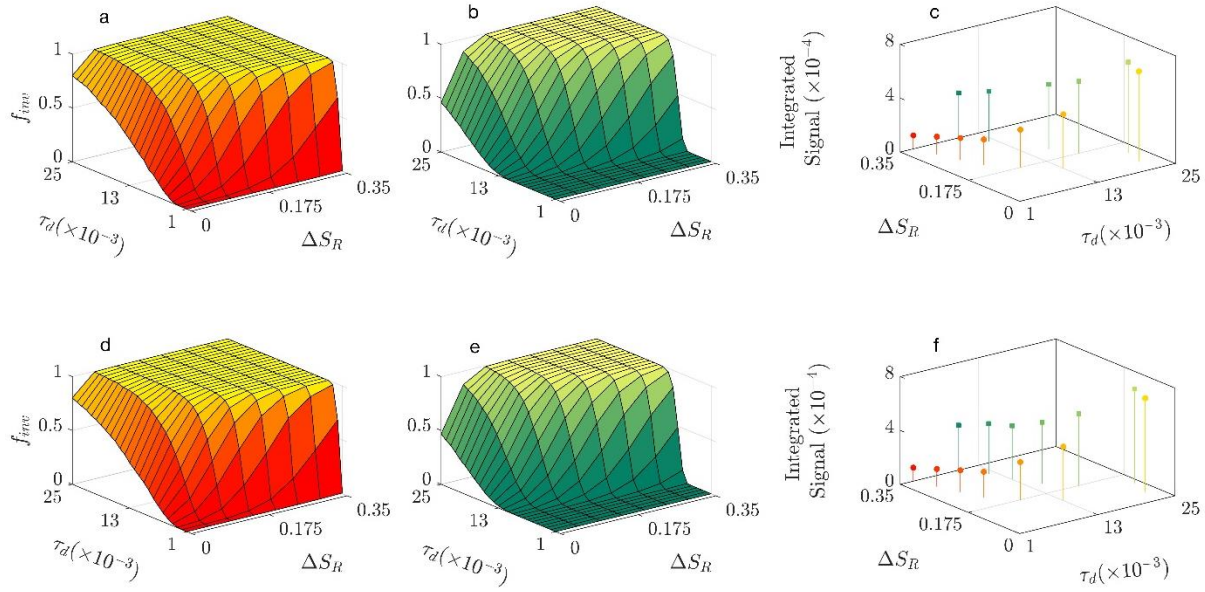

Fig.S1: Effect of resting pulse on the population inversion. The plot of f_{inv} as a function pulse duration (τ_d) and pulse dose (ΔS_R) for the DNFL (fisrt column) and PFL (second column) networks for two different doses of resting pulse ($\Delta S_L = 0.05$ top row, and $\Delta S_L = 0.1$, bottom row). The integrated signal required for 99% population inversion is plotted as a function of τ_d and ΔS_R for two different values of resting pulse (c & f) in the DNFL (circles) and PFL (squares) networks.

ACCEPTED

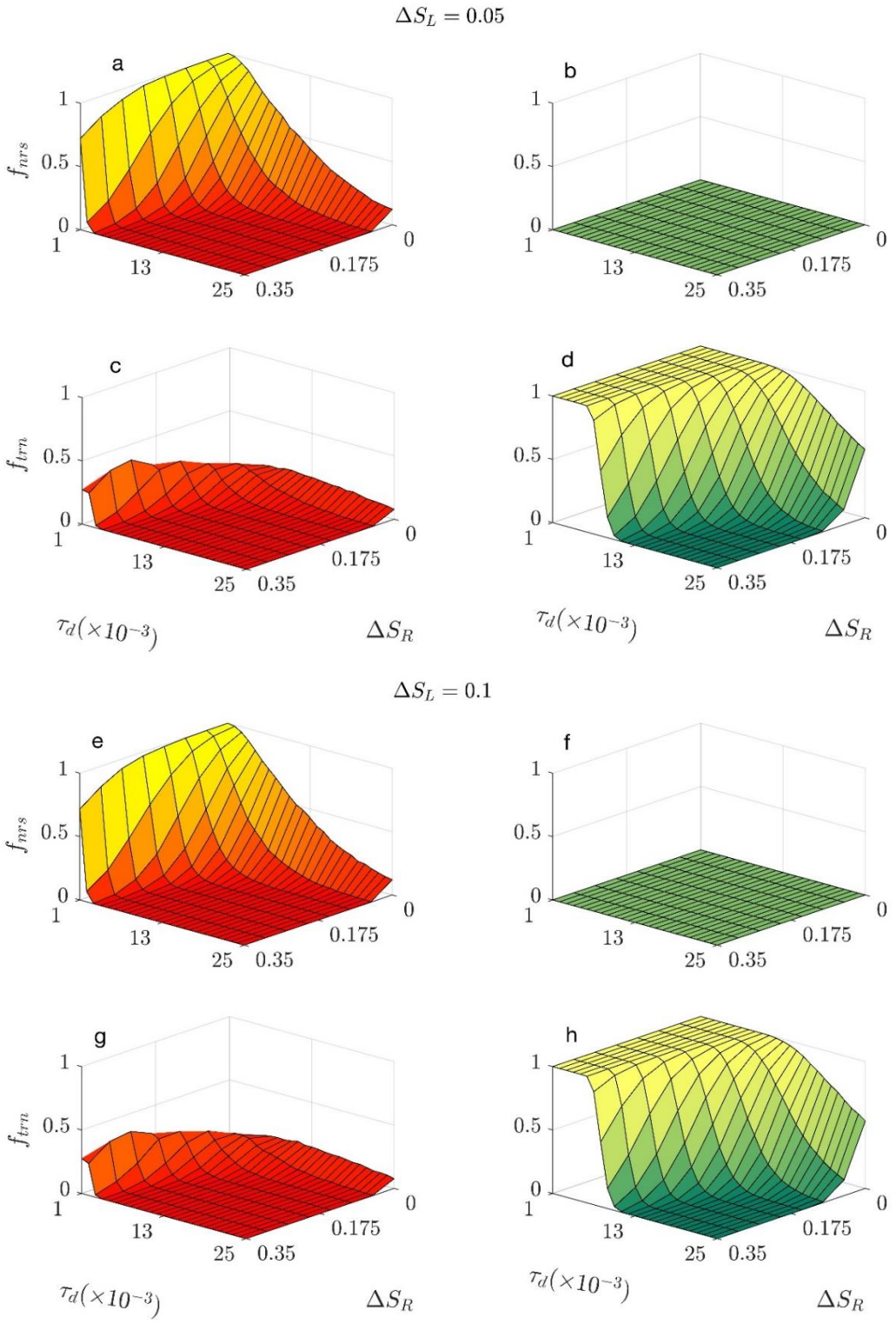

Fig.S2: Effect of resting pulse on the transient dynamics. f_{nrs} and f_{trn} are plotted as a function of τ_d and ΔS_R for the DNFL (a, c, e and f) and PFL (b, d, f and h) networks for different values of resting pulse, $\Delta S_L = 0.05$ (a-d) and $\Delta S_L = 0.1$ (e-h).

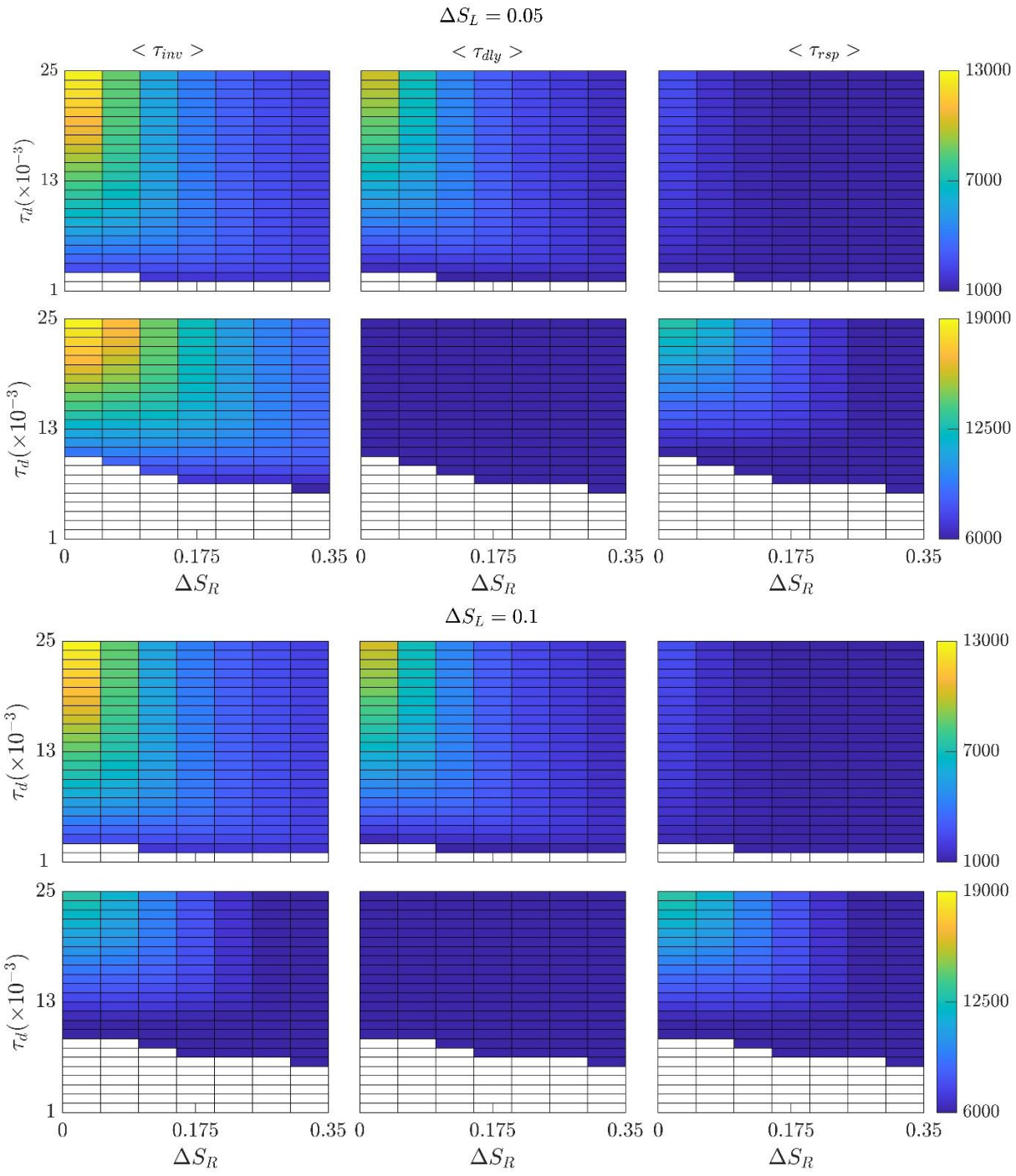

Fig.S3: Effect of resting pulse on the time scales of population inversion. The surface plots of average inversion time ($\langle\tau_{inv}\rangle$), average response time ($\langle\tau_{rsp}\rangle$) and average initial delay time ($\langle\tau_{dly}\rangle$) are presented as a function of τ_d and ΔS_R for the DNFL (1st and 3rd rows) and PFL (2nd and 4th rows) networks at two different values of ΔS_L.

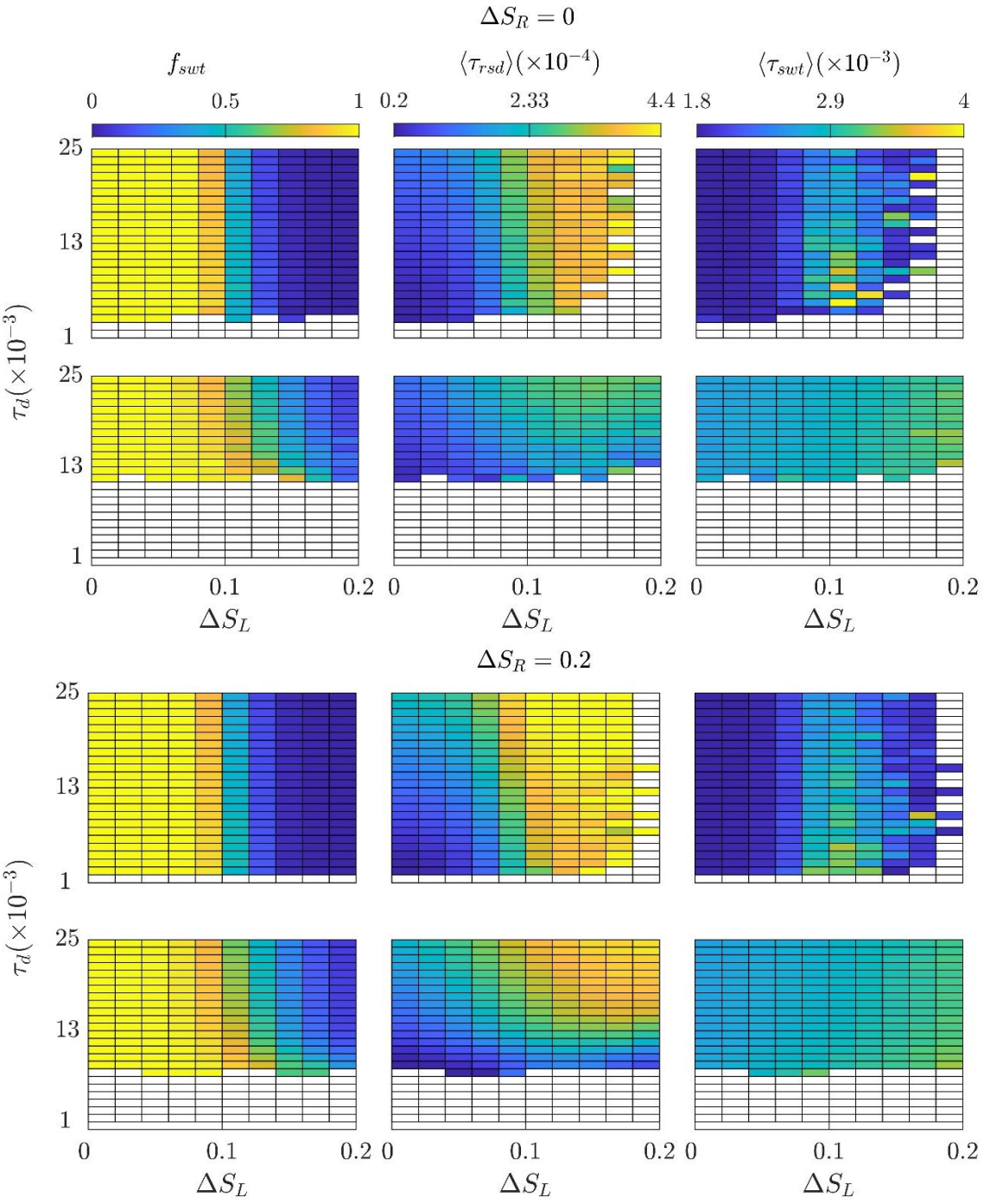

Fig.S4: Effect of pulse amplitude on residence and switching times. The fraction of the population that switches back to the upper steady state (f_{swt}), the average residence time in the lower steady state ($\langle\tau_{rsd}\rangle$) and the average switching time ($\langle\tau_{swt}\rangle$) are plotted as a function of pulse duration (τ_d) and resting pulse (ΔS_L) for the DNFL (1st and 3rd rows) and PFL (2nd and 4th rows) networks. The values of the ΔS_R were 0.0 and 0.2.

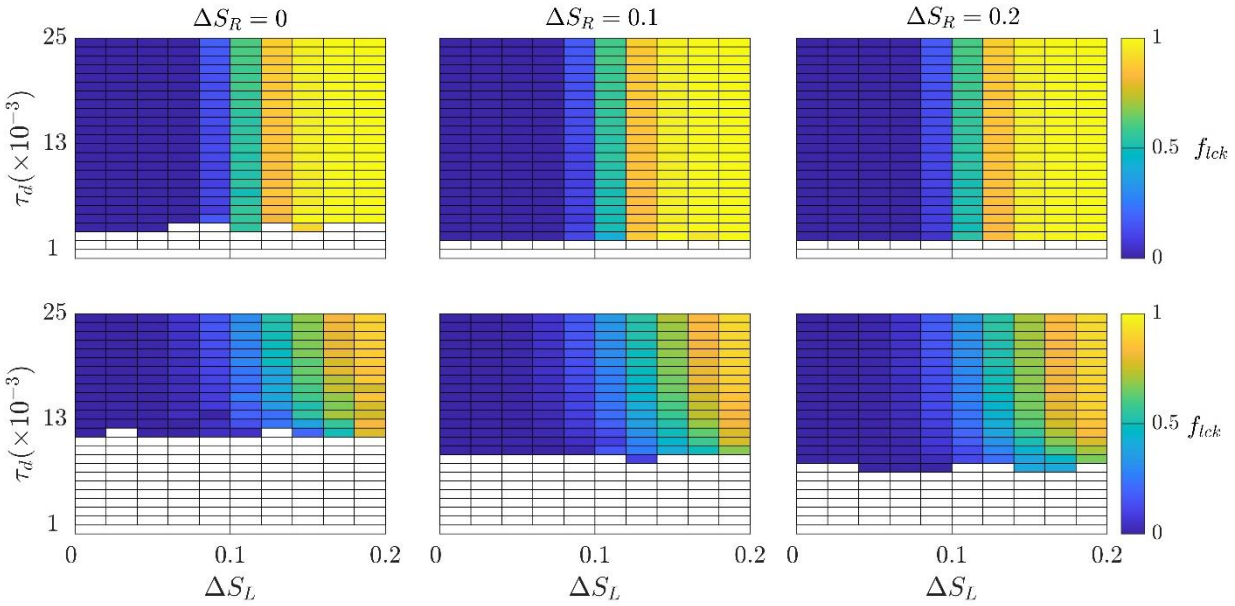

Fig.S5: The effect of pulse amplitude on the population locked in the inverted state. Fraction of cells locked at lower steady state, f_{lck} is plotted as a function of pulse duration (τ_d) and resting pulse (ΔS_L) for the DNFL (top row) and PFL (bottom row) networks for the indicated values of pulse amplitude.

ACCEPTED

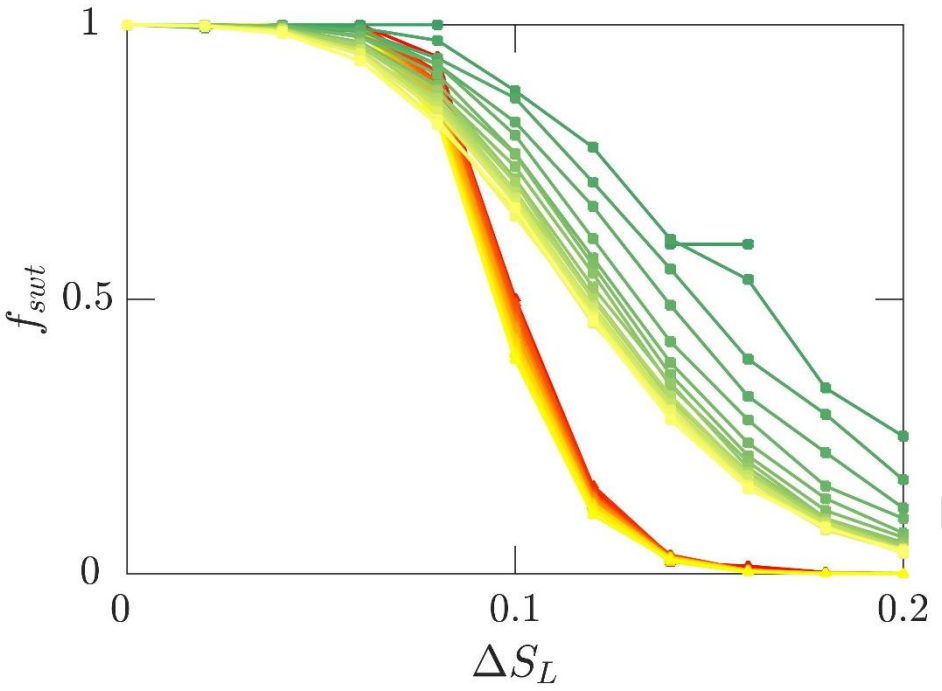

Fig.S6. The fraction of the population that switches back to the upper steady state (f_{swt}) is plotted as a function of resting pulse (ΔS_L) for increasing values of pulse duration, τ_d, in case of DNFL (red to yellow) and PFL (green to yellow) networks. The value of the ΔS_R was 0.2.

ACCEPTED

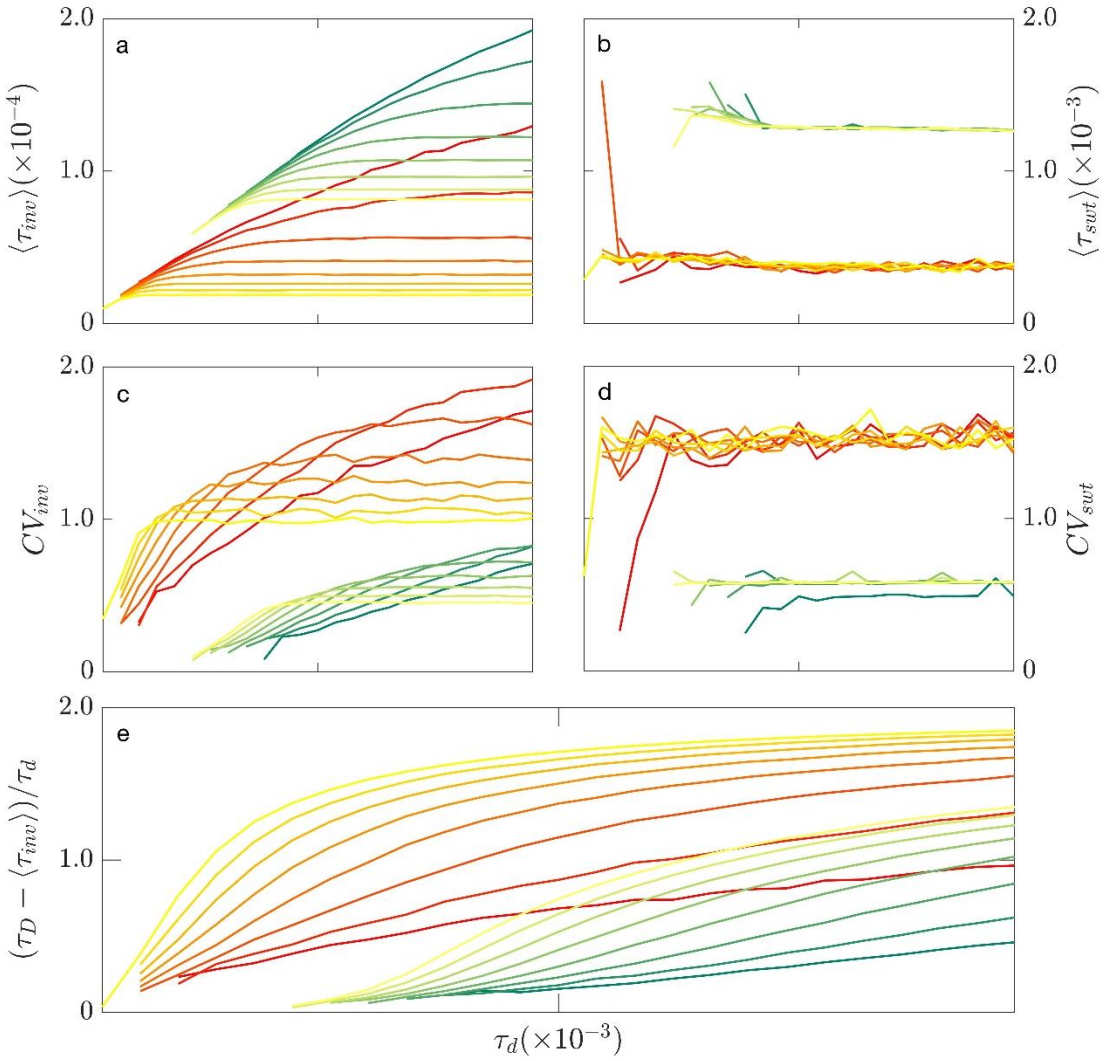

Fig.S7: The comparison of statistical properties of inversion and switching times between the DNFL and PFL networks for different values of pulse dose (a-d). The comparison of relative available time vs. τ_d between the DNFL and PFL networks. Different colors represent different value of dose (ΔS_R) following an increasing trend of red to yellow for the DNFL and green to yellow for the PFL.

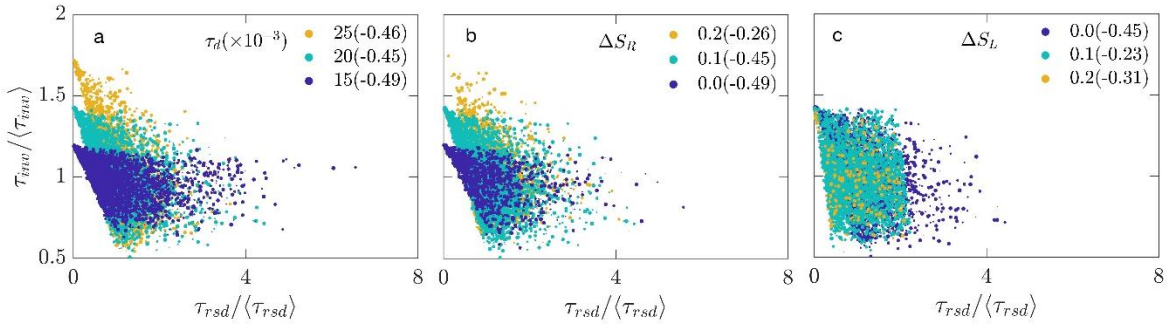

Fig.S8: The correlation between the mean-normalized τ_{inv} and τ_{rsd} times are plotted for the indicated values of pulse duration (a), pulse dose (b) and resting pulse (c) for the PFL network. The values of correlation coefficients are indicated within the parenthesis inside each plot.

ACCEPTED